

Nematic state in CeAuSb₂

S. Seo¹, Xiaoyu Wang², S. M. Thomas¹, M. C. Rahn¹, D. Carmo³, F. Ronning¹, E. D. Bauer¹, R. D. dos Reis³, M. Janoschek^{1,4}, J. D. Thompson¹, R. M. Fernandes⁵ and P. F. S. Rosa¹

¹ Los Alamos National Laboratory - Los Alamos, NM 87545, USA

² James Frank Institute - University of Chicago - Chicago, IL 60615, USA

³ Brazilian Synchrotron Light Laboratory (LNLS) - Campinas - Sao Paulo, Brazil.

⁴ Laboratory for Scientific Developments and Novel Materials - Paul Scherrer Institut - Villigen PSI - Switzerland.

⁵ School of Physics and Astronomy - University of Minnesota - Minneapolis MN 55455, USA

At ambient pressure and zero field, tetragonal CeAuSb₂ hosts stripe antiferromagnetic order at $T_N = 6.3$ K. Here we first show *via* bulk thermodynamic probes and x-ray diffraction measurements that this magnetic order is connected with a structural phase transition to a superstructure which likely breaks C_4 symmetry, thus signaling nematic order. The temperature-field-pressure phase diagram of CeAuSb₂ subsequently reveals the emergence of additional ordered states under applied pressure at a multicritical point. Our phenomenological model supports the presence of a vestigial nematic phase in CeAuSb₂ akin to iron-based high-temperature superconductors; however, superconductivity, if present, remains to be discovered.

I. INTRODUCTION

Heavy-fermion systems, which consist of a lattice of f -electrons that hybridize with the conduction electron sea, host prototypical examples of strongly correlated electronic states [1–4]. In particular, tetragonal Ce-based compounds often reveal novel quantum states of matter in the vicinity of a quantum critical point (QCP) at which a magnetic transition is suppressed to zero temperature by non-thermal parameters, e.g. pressure, magnetic field, or chemical doping [5, 6]. Non-Fermi liquid (NFL) behavior, complex magnetic order, charge order and unconventional superconductivity (SC) are examples of these states, which also have been observed in copper-oxide and iron pnictide high- T_c superconductors, although often accompanied by electronic nematicity – an electronic state that breaks the rotational symmetry of the underlying lattice but not its translational symmetry [7–9]. The origin of the nematic state as well as its role on the superconducting state remains controversial [10]. More recently, evidence for nematicity at high magnetic fields has been found in the heavy-fermion CeRhIn₅ [11], indicating that superconductivity and nematicity also may be intertwined in this class of strongly correlated materials [12]. Recent magnetostriction and nuclear magnetic resonance experiments point to the importance of crystalline electric field (CEF) effects in the putative nematic state of CeRhIn₅ [13, 14].

Ce T Sb₂ (T = transition metal) is also a dense Kondo lattice system with pronounced CEF effects [15, 16]. The magnetic and CEF ground state of Ce T Sb₂ depend on the transition metal T [16, 17], and CeAuSb₂ orders antiferromagnetically below $T_N = 5 - 6.8$ K depending on the occupancy of the Au site [18–20]. Previous x-ray and neutron diffraction measurements showed that CeAuSb₂ crystallizes in a tetragonal crystal structure ($P4/nmm$) [21, 22]. Pressurizing CeAuSb₂ does not suppress T_N to zero temperature, but rather induces new phases hinder-

ing the appearance of a QCP or SC [20]. The nature of the pressure-induced phases in CeAuSb₂ remains an open question, but possibly stems from competing magnetic interactions known to exist in this series of compounds [23]. Unlike pressure, magnetic fields are symmetry breaking and tend to localize $4f$ electrons. In CeAuSb₂, T_N is gradually suppressed by magnetic fields applied along the c -axis and two metamagnetic (MM) transitions are observed at $H_{c1} \sim 2.8$ T and $H_{c2} \sim 5.6$ T at low temperature [18]. The H - T phase diagram constructed by magnetoresistance measurements reveals that both MM transitions are first-order at low temperature and that H_{c2} has a tricritical point at 3.7 K [19]. In addition, a recent neutron diffraction study revealed that at H_{c1} the magnetic structure changes from a single- q striped phase with wave vector $\mathbf{Q}_1 = (\eta, \eta, 1/2)$ [$\eta = 0.136(2)$] to a multi- q (woven or checkered) phase with $\mathbf{Q}_1 = (\eta, \eta, 1/2)$ and $\mathbf{Q}_2 = (\eta, -\eta, 1/2)$ [22]. This ground state competition again stems from competing magnetic interactions, and resembles the single- q to double- q magnetic transition observed in pnictides [24]. Further, striped phases appear to be ubiquitous in strongly correlated systems including manganites, cuprates, nickelates and cobaltites [25–28].

Remarkably, both striped and woven magnetic phases in CeAuSb₂ have 2-fold rotational symmetry in the ab -plane even though the underlying lattice has 4-fold rotational symmetry at high temperatures. As a result, one expects that the lattice will also break tetragonal C_4 symmetry in the presence of magnetoelastic coupling. In fact, in-plane uniaxial pressure experiments show that the magnetic transitions of CeAuSb₂ are sensitive to strain [29, 30]. The situation thus seems analogous to iron-based high- T_c superconductors such as NaFeAs (“111”) and LaFeAsO (“1111”), which share the same $P4/nmm$ space group as CeAuSb₂ [31, 32]. There, the stripe magnetic order is generally preceded by a nematic phase with broken C_4 symmetry of the underlying lattice, in agreement with general theoretical expectations [33–36].

Here we investigate whether such a nematic state exists

in heavy-fermion CeAuSb₂. Bulk thermodynamic probes show the presence of two transitions at about 6.5 K and 6.3 K in CeAuSb₂ at ambient pressure. X-ray diffraction measurements reveal that the development of zero-field striped magnetic order is connected to a structural transition. Our phenomenological model proposes that this structural transition must be a nematic transition at $T_{\text{nem}} \geq T_N$. Our results support the scenario in which CeAuSb₂ hosts a nematic phase that is not intertwined with superconductivity.

II. METHODS

Single crystals of CeAuSb₂ were synthesized by a self-flux method described in Ref. [19]. The highest T_N of 6.8 K is achieved in the electrical resistivity when the crystals are close to being stoichiometric, i.e., an average site occupancy of 100% of Au and residual resistivity ratio (RRR) of about 20. Single crystals were pressurized to 2.66 GPa using a hybrid Be-Cu/NiCrAl clamp-type pressure cell. Daphne oil 7373 was used as a pressure-transmitting medium and lead was used as a manometer [37]. The in-plane electrical resistivity of CeAuSb₂ was measured using a conventional four-probe technique with an LR700 Resistance Bridge in ⁴He and ³He cryostats from 300 K to 0.3 K. Magnetization measurements were performed using a commercial superconducting quantum interference device (SQUID) and the specific heat was measured using a commercial small mass calorimeter that employs a quasi-adiabatic thermal relaxation technique. Thermal expansion along the *c*-axis was measured at atmospheric pressure using a capacitance cell dilatometer with a resolution in $\Delta L/L$ of 10^{-8} . X-ray powder diffraction (XPD) measurements were performed at the X-ray diffraction and spectroscopy (XDS) beamline of the Brazilian Synchrotron Light Laboratory in Campinas, which uses a 4 T superconducting multipolar wiggler source [38]. The XPD patterns were collected at 20 keV in a transmission geometry using an area detector (MAR345). The sample was mounted at the cold finger of an open-cycle He cryostat (base temperature 2.3 K).

III. RESULTS

Specific heat, magnetic susceptibility, and thermal expansion measurements in CeAuSb₂ reveal two closely lying transitions. As shown in Fig. 1(a), and highlighted in the inset of Fig. 1(b), two peaks occur in the specific heat at $T_{\text{nem}} = 6.48$ K and $T_N = 6.33$ K, indicated by arrows. Figure 1(c) shows the temperature dependence of the magnetic susceptibility for $H \parallel [001]$, and the presence of two distinct phase transitions is evident in the derivative $d\chi/dT$ at $T_{\text{nem}} = 6.53$ K and $T_N = 6.33$ K shown in the inset. Figure 1(d) shows the temperature dependence of the *c*-axis length change, $\Delta L_c/L_c$, with an anomaly in the vicinity of 6.5 K. This anomaly is not typical of

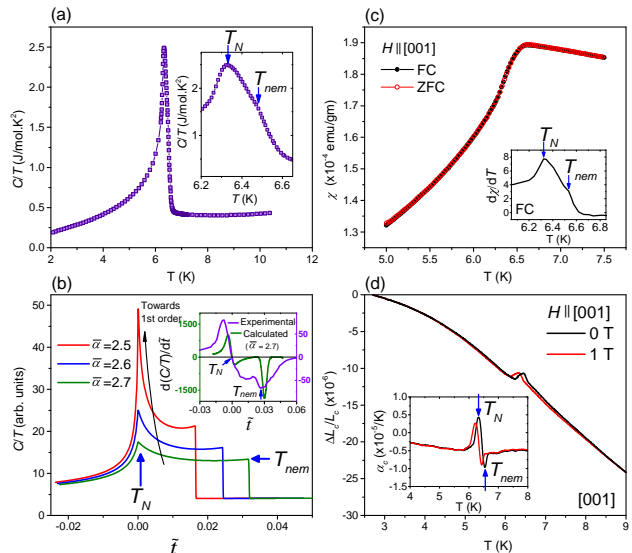


FIG. 1. (a) Specific heat divided by temperature of CeAuSb₂ at ambient pressure. Inset is a magnified view near the peak position. Arrows indicate the transition temperatures T_{nem} and T_N . (b) Calculated C/T versus reduced temperature for fixed anisotropy ζ and various inverse nematic coupling strength $\bar{\alpha}$. Inset gives the derivative of C/T of the experimental data (purple) and of the calculations with $\bar{\alpha} = 2.7$ (green). The theoretical curve was shifted and averaged over disorder for better comparison with the experimental data; details are given in the Supplementary Material. (c) Temperature dependent magnetic susceptibility in an applied field of 1 kOe along the *c*-axis. ZFC (zero-field cooled; open circles) and FC (field-cooled; solid circles) curves show two transitions without hysteresis. The inset plots the derivative $d\chi/dT$. (d) Temperature dependence of the thermal expansion $\Delta L/L$ of CeAuSb₂ along [001] at zero field and 1 T applied along the *c*-axis. The inset gives the thermal expansion coefficient.

purely magnetic phase transitions [39, 40], and the linear thermal-expansion coefficient, $\alpha_c = (1/L_c)(dL_c/dT)$, further reveals a negative peak at $T_{\text{nem}} = 6.55$ K as well as a positive peak at $T_N = 6.33$ K, respectively (see inset of Fig. 1(d)). T_{nem} and T_N decrease together when a field of 1 T is applied, suggesting a strong coupling of the order parameters associated with these transitions. As we will come to below, T_{nem} is associated with a structural transition which likely breaks C_4 symmetry and T_N with a magnetic transition to the single-*q* stripe phase.

X-ray powder diffraction patterns of CeAuSb₂ measured at $T=7$ K and $T=3$ K are shown in Fig. 2. Rietveld refinement of the 7 K data in the published structure [41] provides a satisfactory fit in the $P4/nmm$ cell with lattice parameters $a = 4.3954(2)\text{\AA}$ and $c = 10.318(1)\text{\AA}$. As indicated by the black difference line ($I(3\text{K}) - I(7\text{K})$) in Fig. 2, the intensities of most Bragg peaks change (i.e., increase or decrease) below T_N/T_{nem} , whereas a number of intensities also appear unaffected. Within the limited resolution of this experiment ($\Delta d/d > 10^{-4}$), we observe no evidence for a lattice distortion. As illustrated

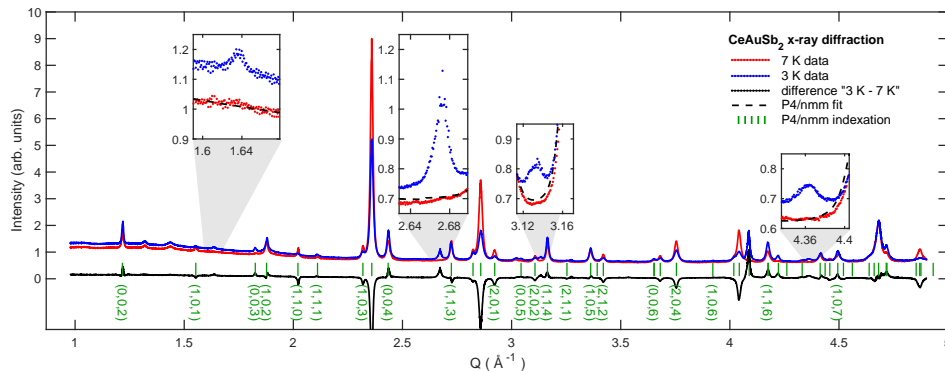


FIG. 2. Synchrotron (20 keV) x-ray powder diffraction patterns of CeAuSb_2 obtained above (7 K, red) and below (3 K, blue) the transitions at $T_{N,\text{nem}}$. The difference pattern (black line) emphasizes significant intensity gains, or losses, at most Bragg positions. Green markers and labels indicate the indexation of these peaks in the high-temperature $P4/nmm$ structure. A lattice distortion is not resolved. Below the structural transition, four additional Bragg peaks are observed (see insets), which are not indexed by the parent phase.

by the insets in Fig. 2, however, four peaks appear at low temperatures which are not indexed in the parent phase and thus confirm that the true symmetry of the low temperature phase of CeAuSb_2 is lower than that of the $P4/nmm$ space group. Due to the powder average and the limited number of observed intensities in the present dataset, the full solution of the low-temperature modulated structure will have to await a single crystal diffraction study. Nevertheless, the absence of nuclear satellite peaks in neutron diffraction measurements [22] suggests that the x-ray diffraction superstructure peaks are due to a modulation of charge density, which is intimately coupled to the magnetic order parameter.

The existence of a magnetic ordered state that breaks a point-group symmetry (i.e., tetragonal symmetry), besides time-reversal symmetry, suggests that the phase transition can happen in two stages [36]: at T_{nem} , tetragonal symmetry is broken, whereas at T_N , time-reversal symmetry is broken. In order to describe these transitions in CeAuSb_2 , we consider a phenomenological model using a stripe magnetic order with a two-component order parameter $\mathbf{m} = (\mathbf{m}_1, \mathbf{m}_2)$, with ordering wavevectors $\mathbf{Q}_1 = (\eta, \eta, 1/2)$ and $\mathbf{Q}_2 = (\eta, -\eta, 1/2)$ for \mathbf{m}_1 and \mathbf{m}_2 , respectively. Note that these two ordering vectors are not equivalent in the $P4/nmm$ group, but are related by a 90° rotation. Up to quartic terms, the Ginzburg-Landau free energy compatible with the symmetries present in CeAuSb_2 is given by:

$$F = \frac{1}{2}r_0(\mathbf{m}_1^2 + \mathbf{m}_2^2) + \frac{u}{4}(\mathbf{m}_1^2 + \mathbf{m}_2^2)^2 - \frac{g}{4}(\mathbf{m}_1^2 - \mathbf{m}_2^2)^2, \quad (1)$$

where $r_0 \propto T - T_N^0$, $u > g > 0$. This is identical to the free energy employed to understand the nematic phase of the pnictides [35]. Here for simplicity we have considered both \mathbf{m}_1 and \mathbf{m}_2 to be real, and that contributions from higher harmonics are neglected. Within a mean-field approximation, at $T < T_N^0$, the free energy is minimized by developing a stripe magnetic order,

with either $\langle \mathbf{m}_1 \rangle$ or $\langle \mathbf{m}_2 \rangle$ becoming non-zero. Such a magnetic order also breaks C_4 symmetry down to C_2 . Therefore, T_N^0 marks a simultaneous second-order nematic and magnetic phase transition. Going beyond mean field analysis and including the effects of magnetic fluctuations, this model generally predicts a nematic transition at $T_{\text{nem}} \geq T_N$, where T_N is the renormalized magnetic transition temperature to the stripe phase [35]. Such a paramagnetic-nematic state is characterized by anisotropic magnetic fluctuations, $\langle \mathbf{m}_1^2 - \mathbf{m}_2^2 \rangle \neq 0$, which spontaneously break the C_4 symmetry of the system even though $\langle \mathbf{m}_1 \rangle = \langle \mathbf{m}_2 \rangle = 0$. The fate of the coupled magnetic-nematic transitions depends on the parameters of the phenomenological model, which in our case are the degree of anisotropy of the magnetic fluctuations and the nematic coupling strength. The former is given by the ratio $\zeta \equiv J_z/J$ between the out-of-plane and in-plane effective exchange interactions, whereas the latter is given by the ratio $\bar{\alpha} \equiv u/g$ of the coefficients of Eq. (1). As shown previously in Ref. [35], for a fixed ζ , large $\bar{\alpha}$ gives two split second-order transitions at $T_{\text{nem}} > T_N$, whereas small $\bar{\alpha}$ gives a simultaneous first-order transition. In the intermediate $\bar{\alpha}$ range, the transitions remain split, but one of them becomes first-order [35] (see Supplementary Material for details). We computed the entropy and heat capacity for a fixed ζ and decreasing $\bar{\alpha}$ towards the critical value $\bar{\alpha}_c$ below which the magnetic transition becomes first-order but remains split from the nematic transition (see Supplementary Materials for details). Figure 1(b) shows the calculated heat capacity C/T as a function of reduced temperature $\tilde{t} \propto (T - T_N)/T_N$. Upon approaching $\bar{\alpha}_c$, the specific heat peak at T_N increases at a faster rate than the jump at T_{nem} , and the separation between the two transition temperatures decreases, signaling the approach of a first-order magnetic transition. In order to compare our model with the experimental result in Fig 1(a), which do not show sharp jumps, we include weak disorder by considering a distribution of T_N^0 values, yield-

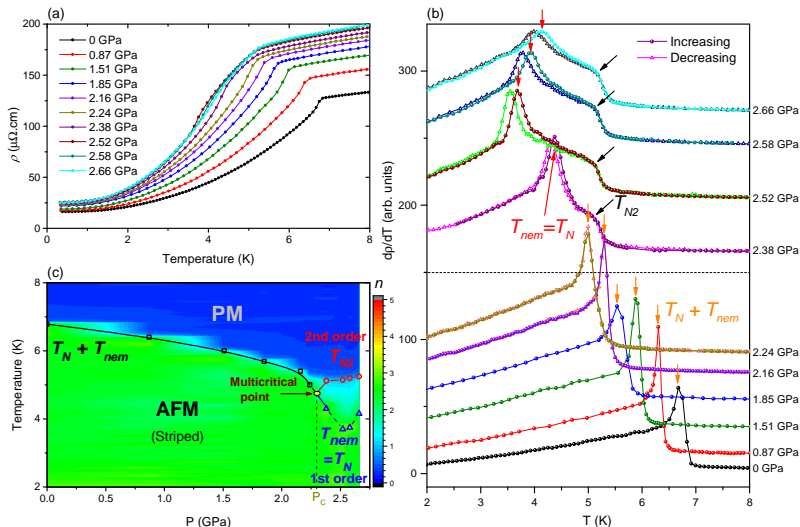


FIG. 3. (a) Temperature dependence of the in-plane electrical resistivity, ρ_{ab} , for CeAuSb₂ at pressures to 2.66 GPa. (b) Temperature derivative of ρ_{ab} under pressure. Data at different pressures are shifted for clarity. Arrows indicate peak positions: orange, black, and red arrows for the $T_N + T_{nem}$, T_{N2} , and $T_{nem} = T_N$, respectively. Above 2.16 GPa, the results from increasing- and decreasing-temperature ramps are indicated by solid and open symbols, respectively. (c) T - P phase diagram of CeAuSb₂ in zero applied field. Colors represent the local exponent, $n = \partial \ln \Delta \rho / \partial \ln T$.

ing a smooth temperature dependence of the derivative of C/T (see inset of Fig. 1(b)). The comparison shows that $d(C/T)/dT = 0$ at T_N and $d(C/T)/dT$ has a minimum at T_{nem} and suggests that CeAuSb₂ at ambient conditions is close to $\bar{\alpha} = 2.7$. Our model predicts that below $\bar{\alpha}_c$, both nematic and magnetic phase transitions become first-order and simultaneous at $T_{nem} = T_N$. As we will come to below, our experimental data under applied pressure suggest that hydrostatic pressure might reduce $\bar{\alpha}$, thus driving the transition first-order and simultaneous.

Now we turn our attention to the field and pressure dependence of the coupled transitions in CeAuSb₂. Figure 3(a) shows the temperature dependence of the in-plane resistivity (ρ_{ab}) of CeAuSb₂ under various pressures up to 2.66 GPa. At ambient pressure, a sharp drop in ρ_{ab} occurs at ~ 6.8 K. As shown in Fig. 3(b), at low pressure a single peak marked by orange arrows occurs in $d\rho/dT$. Within the resolution of these data ($\Delta T \sim 0.08$ K), this single peak likely encloses both T_N and T_{nem} found in C/T , $d\chi/dT$, and $\Delta L/L$. With increasing pressure, $T_N + T_{nem}$ is suppressed to 5 K at 2.24 GPa. Above 2.24 GPa, however, the single peak splits into two peaks in $d\rho/dT$ which are indicated by black and red arrows, respectively. T_{N2} marks a shoulder-like broad peak which increases with increasing pressure and $T_{nem} = T_N$ marks a sharp symmetric peak which decreases up to 2.52 GPa but increases above 2.52 GPa. We will discuss the origin of these transitions below. Above 2.16 GPa, the results from increasing- and decreasing-temperature ramps are shown together in Fig. 3(b), which are indicated by solid and open symbols, respectively. Interestingly, a hysteresis appears at $T_{nem} = T_N$ in $d\rho/dT$, pointing to

a first-order phase transition. Hysteresis is not typical of a naked antiferromagnetic (AFM) transition but rather suggests the development of a multi component state. At T_{N2} and $T_N + T_{nem}$, however, hysteresis is not observed in the resistivity. To shed light on the temperature-pressure phase diagram shown in Fig. 3(c), we turn to the pressure dependence of the initially coupled transitions estimated *via* Ehrenfest relation:

$$\frac{dT_{N/nem}}{dP} = \frac{V_m \Delta \beta}{\Delta C/T} \quad (2)$$

where V_m is the molar volume, $\Delta \beta$ and $\Delta C/T$ are changes of the volume thermal expansion coefficient and the specific heat divided by temperature at the transition. By using the experimental values of β and C/T at ambient pressure, we obtain $dT_N/dP = 0.37$ K/GPa and $dT_{nem}/dP = -0.77$ K/GPa (see supplementary Fig. S3), i.e., T_{nem} would be suppressed with pressure, whereas T_N would be enhanced with pressure. These transitions, however, are coupled at low pressures, and the sum of the calculated dT/dP values (-0.4 K/GPa) is in good agreement with the experimental pressure dependence of coupled transition, $d(T_N + T_{nem})/dP \approx -0.45$ K/GPa. The fact that T_{N2} increases with pressure above the critical pressure suggests that it is associated with a different ordered state not coupled to a tetragonal-symmetry breaking, whose origin will be discussed below.

The temperature-pressure false-color map of the local exponent n of the temperature dependence of ρ_{ab} is shown in Fig. 3(c), where $n = \partial \ln \Delta \rho / \partial \ln T$ and $\Delta \rho = \rho_{ab} - \rho_0 = AT^n$. The contour map in Fig. 3(c) provides a proxy for the magnetic scattering in differ-

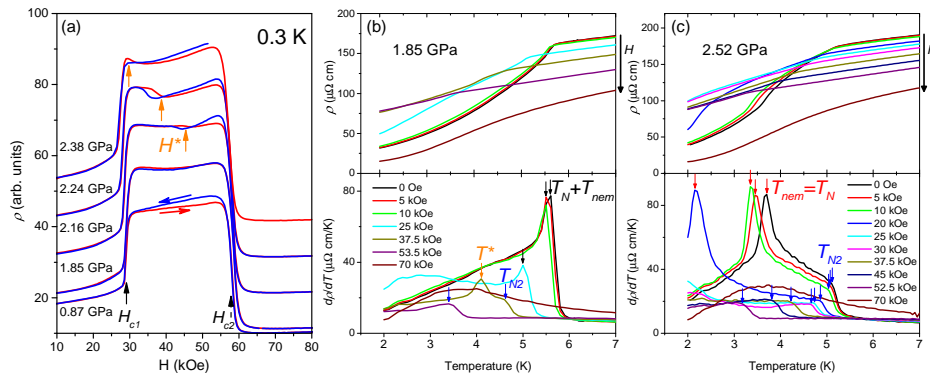


FIG. 4. (a) In-plane electrical resistivity of CeAuSb₂ as a function of magnetic field applied along the *c*-axis at 0.3 K for representative pressures. Magnetoresistance from increasing- and decreasing-field ramps are plotted by red and blue lines, respectively. Data at different pressures are shifted for clarity. (b), (c) Low-temperature in-plane electrical resistivity for various applied magnetic fields at 1.85 GPa and 2.52 GPa. ρ_{ab} and $d\rho/dT$ as a function of temperature are shown in upper and bottom panels, respectively.

ent regions of the phase diagram. Above P_c , the green colored region ($n \approx 2$) below $T_{nem} = T_N$ displays the same behavior as the zero-pressure phase, indicating that the magnetic phase is striped AFM, whereas below T_{N2} the light blue colored region indicates a distinct behavior ($n \approx 1.2$). We will show below in Fig. 5 that the power-law behavior in light blue colored region at high pressure is similar to the behavior of the multi-*q* AFM phase at ambient pressure and high fields. Therefore, our results suggest that the coupled transition at $T_N + T_{nem}$ decouples at P_c into (1) a second-order AFM transition to the multi-*q* phase at T_{N2} and (2) a simultaneous first-order structural and magnetic phase transition to the stripe phase at $T_{nem} = T_N$ due to a finite magnetoelastic coupling. This suggests the existence of a multicritical point at P_c indicated by a yellow circle in Fig. 3(c) at which four phases meet: disordered phase PM, paramagnetic-nematic phase PMnem, antiferromagnetically ordered stripe-nematic phase AFM(S)nem, and antiferromagnetically ordered multi-*q* phase AFM(M).

Evidence for a hysteretic first-order transition is further confirmed in Fig. 4(a), which shows the field dependence of the in-plane resistivity under various pressures, for increasing- and decreasing-field ramps applied along the *c*-axis. At 0.3 K, the first metamagnetic (MM) transition field H_{c1} and the second MM transition field H_{c2} do not change with increasing pressure as shown in Fig. 4(a). At low pressure, the magnetoresistance between H_{c1} and H_{c2} monotonically increases with increasing field, in agreement with Ref. [19]. Above 2.16 GPa, however, a hysteretic step-like anomaly at H^* is observed between H_{c1} and H_{c2} . H^* decreases with increasing pressure and temperature (see supplementary Fig. S4). Figures 4(b) and (c) show the temperature dependence of ρ_{ab} and $d\rho/dT$ at representative pressures for CeAuSb₂ in an applied magnetic field. At 1.85 GPa, the coupled transition at $T_N + T_{nem}$ turns into two transitions at T^* and T_{N2} above H_{c1} . The new field-induced phase transi-

tion at T^* ($H > H_{c1}$) matches the transition at H^* (see supplementary Fig. S7).

Figure 5 displays the temperature-magnetic field false-color map of the local exponent n of ρ_{ab} for representative pressures, where $n = \partial \ln \Delta \rho / \partial \ln T$ and $\Delta \rho = \rho_{ab} - \rho_0 = AT^n$. The contour maps show the presence of two distinct regions in the AFM phase diagrams. The single-*q* region (S) displays a local exponent $n \approx 2$, whereas the multi-*q* region (M) reveals $n \approx 1$ at ambient pressure. At 2.52 GPa, the contour map indicates that the pressure-induced new phase in zero field below T_{N2} is related to the field-driven multi-*q* phase at ambient pressure. In order to understand the origin of T^* and the other phases

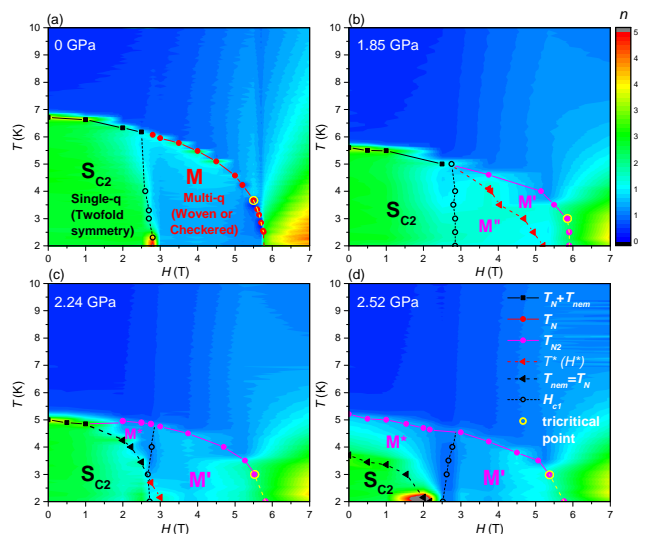


FIG. 5. False-color map of the effective resistivity exponent n in the H - T phase diagram at (a) 0 GPa, (b) 1.85 GPa, (c) 2.24 GPa, and (d) 2.52 GPa. The green region denotes the single-*q* stripe phase (S_{C2}) and the region of light blue denotes the other possible AFM phases (M, M', M'', and M*).

denoted by (M', M'', and M*) under pressure, the underlying magnetic structures will have to be determined by neutron or nuclear magnetic resonance measurements under applied pressure and field. Interestingly, experiments on CeAuSb₂ under uniaxial strain along the [100] direction also suggest additional magnetic phases [29, 30]. Finally, we note that the tricritical point of H_{c2} is not suppressed to zero temperature with pressure (see supplementary information).

IV. DISCUSSION

Striped magnetic phases are ubiquitous in strongly correlated materials [25, 28, 42, 43], and unconventional superconductivity is arguably intertwined with spin and charge stripe correlations in the copper oxides and iron-based materials [26]. Superconductivity, however, is absent in e.g. nickel oxides, which also host a stripe pattern within the NiO₂ planes analogous to the CuO₂ planes in copper oxides [27]. Here we show that the f -electron system CeAuSb₂ also supports a nematic state in the absence of superconductivity. Though nematicity may boost Cooper pairing in the iron-based superconductors, nematic fluctuations may be weak in CeAuSb₂ due to the first-order nature of the nematic transition and the change in the ground-state wavefunction of the system at P_c . Previous pressure work revealed that two energy scales, one associated with Kondo coherence and the other with crystalline electric field (CEF) splitting become similar at P_c . As a result, wave functions of the excited crystal-field levels become admixed into the ground state, hindering formation of a fully Kondo coherent ground state yet allowing new magnetic orders which lead to a magnetic state that persists to over 4 GPa [20]. Because of the competing magnetic interactions known to be present in the class of localized materials, various magnetic orders compete under pressure and magnetic field. The family member CeAgSb₂ also shows a new magnetic phase above $P_c \sim 2.7$ GPa and T_{max} exhibits unexpected negative pressure dependence above P_c which may be due to the influence of a low-

lying CEF level $\Delta_1 \sim 50$ K [40, 44]. Inelastic and elastic neutron scattering studies could shed light on the relation between new magnetic phases and CEF admixture under applied pressure and magnetic field.

V. CONCLUSIONS

In summary, we have constructed the temperature-magnetic field phase diagrams of CeAuSb₂ under applied pressure. Bulk thermodynamic probes reveal two closely lying phase transitions at $T_N = 6.3$ K and $T_{nem} = 6.5$ K, and x-ray diffraction measurements verify that striped magnetic order is connected to a structural phase transition at ambient pressure. Our theoretical model suggests that stripe magnetic order is preceded by a nematic phase in CeAuSb₂. The discovery of a putative nematic phase in an f -electron material at zero magnetic field provides an unexplored framework for nematicity, though superconductivity if present remains to be discovered.

ACKNOWLEDGMENTS

Work at Los Alamos was performed under the auspices of the U.S. Department of Energy, Office of Basic Energy Sciences, Division of Materials Science and Engineering. S.S. acknowledges a Directors Postdoctoral Fellowship through the Laboratory Directed Research & Development program. Scanning electron microscope and energy dispersive X-ray measurements were performed at the Center for Integrated Nanotechnologies, an Office of Science User Facility operated for the U.S. Department of Energy (DOE) Office of Science. Theory work (R.M.F.) was supported by the U.S. Department of Energy, Office of Science, Basic Energy Sciences, under Award No. DE-SC0012336. XW is supported by the University of Chicago Materials Research Science and Engineering Center, which is funded by the National Science Foundation under award number DMR-1420709. R.D. dos Reis and D. Carmo thanks the financial support from the Brazilian agencies CAPES and FAPESP (Grants 2018/00823-0 and 2018/22883-5).

-
- [1] G. R. Stewart, Heavy-fermion systems, Rev. Mod. Phys. **56**, 755 (1984).
 - [2] Z. Fisk, D. W. Hess, C. J. Pethick, D. Pines, J. L. Smith, J. D. Thompson, and J. O. Willis, Heavy-Electron Metals: New Highly Correlated States of Matter, Science **239**, 33 (1988).
 - [3] P. Coleman, Heavy Fermions: Electrons at the Edge of Magnetism, in *Handbook of Magnetism and Advanced Magnetic Materials* (John Wiley & Sons, Ltd, Chichester, UK, 2007) pp. 95–148.
 - [4] P. Coleman, Heavy Fermions: Dimensions are critical, Nat. Mater. **11**, 185 (2012).
 - [5] H. v. Löhneysen, A. Rosch, M. Vojta, and P. Wölfle, Fermi-liquid instabilities at magnetic quantum phase transitions, Rev. Mod. Phys. **79**, 1015 (2007).
 - [6] G. R. Stewart, Non-Fermi-liquid behavior in d - and f -electron metals, Rev. Mod. Phys. **73**, 797 (2001).
 - [7] T. Shibauchi, A. Carrington, and Y. Matsuda, A Quantum Critical Point Lying Beneath the Superconducting Dome in Iron Pnictides, Annu. Rev. Condens. Matter Phys. **5**, 113 (2014).
 - [8] E. Fradkin, S. A. Kivelson, M. J. Lawler, J. P. Eisenstein, and A. P. Mackenzie, Nematic Fermi Fluids in Condensed Matter Physics, Annu. Rev. Condens. Matter Phys. **1**,

- 153 (2010).
- [9] R. M. Fernandes, A. V. Chubukov, and J. Schmalian, What drives nematic order in iron-based superconductors?, *Nat. Phys.* **10**, 97 (2014).
- [10] S. Lederer, Y. Schattner, E. Berg, and S. A. Kivelson, Superconductivity and non-Fermi liquid behavior near a nematic quantum critical point, *Proc. Natl. Acad. Sci.* **114**, 4905 (2017).
- [11] F. Ronning, T. Helm, K. R. Shirer, M. D. Bachmann, L. Balicas, M. K. Chan, B. J. Ramshaw, R. D. McDonald, F. F. Balakirev, M. Jaime, E. D. Bauer, and P. J. W. Moll, Electronic in-plane symmetry breaking at field-tuned quantum criticality in CeRhIn_5 , *Nature* **548**, 313 (2017).
- [12] R. Okazaki, T. Shibauchi, H. J. Shi, Y. Haga, T. D. Matsuda, E. Yamamoto, Y. Onuki, H. Ikeda, and Y. Matsuda, Rotational Symmetry Breaking in the Hidden-Order Phase of URu_2Si_2 , *Science* **331**, 439 (2011).
- [13] P. F. S. Rosa, S. M. Thomas, F. F. Balakirev, E. D. Bauer, R. M. Fernandes, J. D. Thompson, F. Ronning, and M. Jaime, Enhanced Hybridization Sets the Stage for Electronic Nematicity in CeRhIn_5 , *Phys. Rev. Lett.* **122**, 016402 (2019).
- [14] G. G. Lesseux, H. Sakai, T. Hattori, Y. Tokunaga, S. Kambe, P. L. Kuhns, A. P. Reyes, J. D. Thompson, P. G. Pagliuso, and R. R. Urbano, Orbitally defined field-induced electronic state in a Kondo lattice, (2019), arXiv:1905.02861.
- [15] Y. Muro, N. Takeda, and M. Ishikawa, Magnetic and transport properties of dense Kondo systems, CeTSb_2 ($T=\text{Ni, Cu, Pd and Ag}$), *J. Alloys Compd.* **257**, 23 (1997).
- [16] A. Thamizhavel, T. Takeuchi, T. Okubo, M. Yamada, R. Asai, S. Kirita, A. Galatanu, E. Yamamoto, T. Ebihara, Y. Inada, R. Settai, and Y. Onuki, Anisotropic electrical and magnetic properties of CeTSb_2 ($T=\text{Cu, Au, Ni}$) single crystals, *Phys. Rev. B* **68**, 054427 (2003).
- [17] G. André, F. Bourée, M. Kolenda, B. Leśniewska, A. Oleś, and A. Szytuła, Magnetic structures of RAgSb_2 compounds, *Physica B* **292**, 176 (2000).
- [18] L. Balicas, S. Nakatsuji, H. Lee, P. Schlottmann, T. P. Murphy, and Z. Fisk, Magnetic field-tuned quantum critical point in CeAuSb_2 , *Phys. Rev. B* **72**, 064422 (2005).
- [19] L. Zhao, E. A. Yelland, J. A. N. Bruin, I. Sheikin, P. C. Canfield, V. Fritsch, H. Sakai, A. P. Mackenzie, and C. W. Hicks, Field-temperature phase diagram and entropy landscape of CeAuSb_2 , *Phys. Rev. B* **93**, 195124 (2016).
- [20] S. Seo, V. A. Sidorov, H. Lee, D. Jang, Z. Fisk, J. D. Thompson, and T. Park, Pressure effects on the heavy-fermion antiferromagnet CeAuSb_2 , *Phys. Rev. B* **85**, 205145 (2012).
- [21] H. Flandorfer, O. Sologub, C. Godart, K. Hiebl, A. Leithe-Jasper, P. Rogl, and H. Noël, On the cerium valence in ternary compounds CeMSb_2 and CeM'Bi_2 ; $M=\text{Mn, Fe, Co, Ni, Cu, Zn, Pd, Ag, Au}$ and $M'=\text{Ni, Cu, Zn, Ag}$, *Solid State Commun.* **97**, 561 (1996).
- [22] G. G. Marcus, D.-J. Kim, J. A. Tutmaher, J. A. Rodriguez-Rivera, J. O. Birk, C. Niedermeyer, H. Lee, Z. Fisk, and C. L. Broholm, Multi- q Mesoscale Magnetism in CeAuSb_2 , *Phys. Rev. Lett.* **120**, 097201 (2018).
- [23] C. Adriano, P. F. S. Rosa, C. B. R. Jesus, J. R. L. Mardegan, T. M. Garitezi, T. Grant, Z. Fisk, D. J. Garcia, A. P. Reyes, P. L. Kuhns, R. R. Urbano, C. Giles, and P. G. Pagliuso, Physical properties and magnetic structure of the intermetallic CeCuBi_2 compound, *Phys. Rev. B* **90**, 235120 (2014).
- [24] J. M. Allred, K. M. Taddei, D. E. Bugaris, M. J. Krogstad, S. H. Lapidus, D. Y. Chung, H. Claus, M. G. Kanatzidis, D. E. Brown, J. Kang, R. M. Fernandes, I. Eremin, S. Rosenkranz, O. Chmaissem, and R. Osborn, Double-Q spin-density wave in iron arsenide superconductors, *Nat. Phys.* **12**, 493 (2016).
- [25] S. Mori, C. H. Chen, and S.-W. Cheong, Pairing of charge-ordered stripes in $(\text{La,Ca})\text{MnO}_3$, *Nature* **392**, 473 (1998).
- [26] J. M. Tranquada, B. J. Sternlieb, J. D. Axe, Y. Nakamura, and S. Uchida, Evidence for stripe correlations of spins and holes in copper oxide superconductors, *Nature* **375**, 561 (1995).
- [27] C. H. Chen, S.-W. Cheong, and A. S. Cooper, Charge modulations in $\text{La}_{2-x}\text{Sr}_x\text{NiO}_{4+y}$: Ordering of polarons, *Phys. Rev. Lett.* **71**, 2461 (1993).
- [28] T. Vogt, P. M. Woodward, P. Karen, B. A. Hunter, P. Henning, and A. R. Moodenbaugh, Low to High Spin-State Transition Induced by Charge Ordering in Antiferromagnetic YBaCo_2O_5 , *Phys. Rev. Lett.* **84**, 2969 (2000).
- [29] J. Park, H. Sakai, O. Erten, A. P. Mackenzie, and C. W. Hicks, Effect of applied orthorhombic lattice distortion on the antiferromagnetic phase of CeAuSb_2 , *Phys. Rev. B* **97**, 024411 (2018).
- [30] J. Park, H. Sakai, A. P. Mackenzie, and C. W. Hicks, Effect of uniaxial stress on the magnetic phases of CeAuSb_2 , *Phys. Rev. B* **98**, 024426 (2018).
- [31] M. D. Lumsden and A. D. Christianson, Magnetism in Fe-based superconductors, *J. Phys.: Condens. Matter* **22**, 203203 (2010).
- [32] C. W. Chu, F. Chen, M. Gooch, A. M. Guloy, B. Lorenz, B. Lv, K. Sasmal, Z. J. Tang, J. H. Tapp, and Y. Y. Xue, The synthesis and characterization of LiFeAs and NaFeAs , *Physica C* **469**, 326 (2009).
- [33] C. Xu, M. Müller, and S. Sachdev, Ising and spin orders in the iron-based superconductors, *Phys. Rev. B* **78**, 020501(R) (2008).
- [34] C. Fang, H. Yao, W.-F. Tsai, J.P. Hu, and S. A. Kivelson, Theory of electron nematic order in LaFeAsO , *Phys. Rev. B* **77**, 224509 (2008).
- [35] R. M. Fernandes, A. V. Chubukov, J. Knolle, I. Eremin, and J. Schmalian, Preemptive nematic order, pseudogap, and orbital order in the iron pnictides, *Phys. Rev. B* **85**, 024534 (2012).
- [36] R. M. Fernandes, P. P. Orth, and J. Schmalian, Intertwined Vestigial Order in Quantum Materials: Nematicity and Beyond, *Annu. Rev. Condens. Matter Phys.* **10**, 133 (2019).
- [37] A. Eiling and J. S. Schilling, Pressure and temperature dependence of electrical resistivity of Pb and Sn from 1-300K and 0-10 GPa-use as continuous resistive pressure monitor accurate over wide temperature range; superconductivity under pressure in Pb, Sn and In, *J. Phys. F: Metal Phys.* **11**, 623 (1981).
- [38] F. A. Lima, M. E. Saleta, R. J. S. Pagliuca, M. A. Eleotério, R. D. Reis, J. Fonseca Júnior, B. Meyer, E. M. Bittar, N. M. Souza-Neto, and E. Granado, XDS: a flexible beamline for X-ray diffraction and spectroscopy at the Brazilian synchrotron, *J. Synchrotron Rad.* **23**, 1538 (2016).

- [39] T. Takeuchi, T. Inoue, K. Sugiyama, D. Aoki, Y. Tokiwa, Y. Haga, K. Kindo, and Y. Onuki, Magnetic and Thermal Properties of CeIrIn₅ and CeRhIn₅, *J. Phys. Soc. Jpn.* **70**, 877 (2001).
- [40] T. Takeuchi, A. Thamizhavel, T. Okubo, M. Yamada, N. Nakamura, T. Yamamoto, Y. Inada, K. Sugiyama, A. Galatanu, E. Yamamoto, K. Kindo, T. Ebihara, and Y. Onuki, Anisotropic, thermal, and magnetic properties of CeAgSb₂: Explanation via a crystalline electric field scheme, *Phys. Rev. B* **67**, 064403 (2003).
- [41] O. Sologub, K. Hiebl, P. Rogl, H. Noël, and O. Bodak, On the crystal structure and magnetic properties of the ternary rare earth compounds RETSb₂ with RE=rare earth and T=Ni, Pd, Cu and Au, *J. Alloys Compd.* **210**, 153 (1994).
- [42] D. D. Khalyavin, D. N. Argyriou, U. Amann, A. A. Yaremchenko, and V. V. Kharton, Low-temperature behavior of YBaCo₂O_{5.5}: Coexistence of two spin-state ordered phases, *Phys. Rev. B* **77**, 064419 (2008).
- [43] K. Knizek, Z. Jirak, E. Pollert, F. Zounova, and S. Vratislav, Structure and magnetic properties of Pr_{1-x}Sr_xMnO₃ perovskites, *J. Solid State Chem.* **100**, 292 (1992).
- [44] V. A. Sidorov, E. D. Bauer, N. A. Frederick, J. R. Jeffries, S. Nakatsuji, N. O. Moreno, J. D. Thompson, M. B. Maple, and Z. Fisk, Magnetic phase diagram of the ferromagnetic Kondo-lattice compound CeAgSb₂ up to 80 kbar, *Phys. Rev. B* **67**, 224419 (2003).